2-20-2018

Electron effective mass in In0.33Ga0.67N determined by mid- infrared optical Hall effect

Nerijus Armakavicius
Linkoping University

Vallery Stanishev
Linkoping University

Sean Knight
University of Nebraska-Lincoln

Mathias Schubert
Linkoping University & University of Nebraska-Lincoln & Leibniz Institute for Polymer Research, mschubert4@unl.edu

Vanya Darakchieva
Linkoping University

Electron effective mass in $In_{0.33}Ga_{0.67}N$ determined by mid-infrared optical Hall effect

Nerijus Armakavicius,[1] Vallery Stanishev,[1] Sean Knight,[2] Philipp Kühne,[1] Mathias Schubert,[1,2,3] and Vanya Darakchieva[1]
[1]*Terahertz Materials Analysis Center, Department of Physics, Chemistry and Biology IFM, Linköping University, SE-58183 Linköping, Sweden*
[2]*Department of Electrical and Computer Engineering and Center for Nanohybrid Functional Materials, University of Nebraska-Lincoln, 68588 Lincoln, Nebraska, USA*
[3]*Leibniz Institute for Polymer Research, 01069 Dresden, Germany*

(Received 5 December 2017; accepted 29 January 2018; published online 20 February 2018)

Mid-infrared optical Hall effect measurements are used to determine the free charge carrier parameters of an unintentionally doped wurtzite-structure *c*-plane oriented $In_{0.33}Ga_{0.67}N$ epitaxial layer. Room temperature electron effective mass parameters of $m_{\perp}^{*} = (0.205 \pm 0.013)\, m_0$ and $m_{\parallel}^{*} = (0.204 \pm 0.016)\, m_0$ for polarization perpendicular and parallel to the *c*-axis, respectively, were determined. The free electron concentration was obtained as $(1.7 \pm 0.2) \times 10^{19}\,\mathrm{cm}^{-3}$. Within our uncertainty limits, we detect no anisotropy for the electron effective mass parameter and we estimate the upper limit of the possible effective mass anisotropy as 7%. We discuss the influence of conduction band nonparabolicity on the electron effective mass parameter as a function of In content. The effective mass parameter is consistent with a linear interpolation scheme between the conduction band mass parameters in GaN and InN when the strong nonparabolicity in InN is included. The $In_{0.33}Ga_{0.67}N$ electron mobility parameter was found to be anisotropic, supporting previous experimental findings for wurtzite-structure GaN, InN, and $Al_xGa_{1-x}N$ epitaxial layers with *c*-plane growth orientation. *Published by AIP Publishing.* https://doi.org/10.1063/1.5018247

Variation of the indium content in wurtzite-structure $In_xGa_{1-x}N$ permits tuning its bandgap from the near-infrared (NIR; InN) to the ultraviolet (UV; GaN) spectral range.[1] Device heterostructures employing low-In content $In_xGa_{1-x}N$ alloys ($x < 0.3$) are widely used in blue light emitting diodes, laser diodes, and vertical-cavity surface-emitting lasers. On the other hand, higher In content ($x > 0.3$) $In_xGa_{1-x}N$ optoelectronic devices for operation at long wavelengths are still emerging. The high electron saturation drift velocity of the two dimensional electron gas in $In_xGa_{1-x}N$ ($\sim 2 \times 10^7\,\mathrm{cm\,s}^{-1}$) makes the material also promising for high frequency and high power electronic switch and transistor applications.[2] Knowledge of free charge carrier properties of $In_xGa_{1-x}N$ alloys and their dependencies on carrier density and In content is a prerequisite for device design and operation and for developing new device architectures. However, reports on electron effective mass, concentration, and mobility parameters in $In_xGa_{1-x}N$ are scarce.

Density functional tight binding calculations predict nearly linear variation of the electron effective mass parameter in wurtzite-structure $In_xGa_{1-x}N$ as a function of In content with a small bowing parameter of 2.27×10^{-3}.[3] Cyclotron resonance and Shubnikov-de Haas measurements, which can typically be used to experimentally determine the effective mass, require high mobility parameters and thus low temperatures and/or very high magnetic fields.[4] Alloy disorder and relatively high density of defects in alloyed thin films typically reduce the mobility parameters compared to the binary compounds rendering Cyclotron resonance and Shubnikov-de Haas measurements inapplicable to currently available $In_xGa_{1-x}N$ materials. The determination of free charge carrier effective mass at room temperature or higher (under device operation condition) temperature is still a challenging task. There are only a few reports which estimate experimentally the effective mass parameters in $In_xGa_{1-x}N$.[5,6] Eljarrat *et al.* estimated an isotropic average of the electron effective mass parameter between 0.14 m_0 and 0.16 m_0 (m_0 is the free electron mass) for multilayer quantum well structures of $In_{0.05}Ga_{0.95}N$ and $In_{0.2}Ga_{0.8}N$ layers using a numerical Kramers-Kronig extension of electron energy loss spectra. Yadav *et al.* investigated polycrystalline $In_xGa_{1-x}N$ layers and estimated isotropically averaged electron effective mass parameters for In content from 0.4 to 1 combining parameters obtained from electrical Hall effect and optical reflectivity measurements.[5] The reported values vary between 0.13 m_0 and 0.42 m_0 and carry large uncertainty limits of more than 50%. Furthermore, values determined from the measured plasma frequencies and the estimated energies of Burstein-Moss shifts assuming parabolic bands differ substantially among the reported set.[5]

The conduction band in the vicinity of the Γ point of the Brillouin zone of InN, and free electron concentrations from $10^{17}\,\mathrm{cm}^{-3}$ to $10^{19}\,\mathrm{cm}^{-3}$, exhibits nonparabolicity.[7] Thus, the electron effective mass in InN increases with increasing free electron concentration.[8] It was shown using optical Hall effect (OHE) measurements that the InN electron effective mass parameter increases by almost a factor of two for an electron concentration of $10^{19}\,\mathrm{cm}^{-3}$ compared to the respective value at the conduction band minimum.[9] On the other hand, the electron effective mass in GaN was shown to be constant for free electron concentrations up to the low $10^{20}\,\mathrm{cm}^{-3}$ range, and hence, the GaN conduction band can

be considered to be parabolic in the vicinity of the Γ point.[10] Due to the uniaxial symmetry of the wurtzite crystal structure, the electron effective mass parameter at the conduction band minimum in InN is anisotropic with $m_{\perp}^{*} = 0.050\, m_0$ and $m_{\parallel}^{*} = 0.037\, m_0$.[9] With increasing carrier concentration, the anisotropy vanishes.[9] For GaN, the effective mass parameter at the conduction band minimum exhibits negligible anisotropy below 1% with $m_{\perp}^{*} = (0.237 \pm 0.006)\, m_0$, $m_{\parallel}^{*} = (0.228 \pm 0.008)\, m_0$.[11] With increasing carrier concentration, the small anisotropy remains.[10] Hence, conduction band nonparabolicity and anisotropy are anticipated in $In_xGa_{1-x}N$ alloys, which may vary as a function of the In content. To this end, no accurate effective mass and anisotropy determination has been reported yet for any In content $0 < x < 1$.

Measurements of the optical Hall effect (OHE) by generalized ellipsometry provide independent access to the free charge carrier concentration, mobility, and effective mass parameters, including their anisotropy, in a contactless manner, and data analysis does not require prior knowledge of band curvature and bandgap parameters.[9,12,13] The OHE can be measured in electrically conductive samples in the presence of an external magnetic field when electromagnetic waves within the mid-infrared (MIR) to terahertz frequency spectral regions interact with the free charge carriers within the sample. The OHE is the high frequency analog to the classical Hall effect and describes optical birefringence due to the motion of free charge carriers under the influence of the Lorentz force. Further details about OHE can be found in Refs. 12 and 13 and references therein.

Ellipsometric data are analyzed using an optical model containing a set of layers each defined by its complex model dielectric function (MDF) and layer thickness parameter. The analysis is performed by fitting parameterized MDFs of all sample constituents (substrate, epilayer) and layer thickness parameters through a stratified optical model to the experimental data. Optical model parameters are varied using regression algorithms until the best match between model and all experimental datasets is achieved.[13]

In this work, we determine the electron effective mass, mobility, and concentration parameters of wurtzite $In_{0.33}Ga_{0.67}N$ using mid-infrared (MIR)-OHE measurements. We discuss the results on the electron effective mass parameter in terms of In content and free electron concentration dependence and estimate the upper limit of the electron effective mass anisotropy that may remain hidden within our present experimental error bars.

An $In_{0.33}Ga_{0.67}N$ layer with a nominal thickness of 300 nm was grown on an AlN template layer on a *c*-plane sapphire (α-Al_2O_3) substrate by molecular beam epitaxy. Both AlN and $In_{0.33}Ga_{0.67}N$ epilayers have a wurtzite crystal structure with their *c*-axes perpendicular to the sample surface. The In content was determined using X-ray diffraction measurements. MIR-spectroscopic ellipsometry (SE) measurements were performed without the external magnetic field at angles of incidence of 55° and 65° using a commercial Fourier transform-based spectroscopic ellipsometer (IR-VASE, J.A. Woollam Co., Inc.), operating in polarizer-sample-compensator-analyzer arrangement, in the spectral range of 300–1200 cm^{-1} with a resolution of 1 cm^{-1}. MIR-OHE measurements were performed within the spectral range of 800–1100 cm^{-1} with a resolution of 1 cm^{-1} and at an angle of incidence of 45° using a custom-built Fourier transform-based generalized ellipsometer system operating in the polarizer-sample-rotating analyzer arrangement.[14] The MIR-OHE measurements were performed at magnetic field strengths ($\vec{\boldsymbol{B}}$) of –6 T, 0 T, and 6 T with the magnetic field vector oriented parallel to the incoming beam. The optical response of the sample was recorded in terms of Ψ and Δ for the MIR-SE and in terms of Mueller matrix spectra $\mathbf{M}(\vec{\boldsymbol{B}})$ for the MIR-OHE measurements.[14] All measurements were performed at room temperature.

We employed the following optical model for the data analysis: surface-charge-depleted $In_{0.33}Ga_{0.67}N$/conductive $In_{0.33}Ga_{0.67}N$/AlN/sapphire. Here, we note that the presence of the depletion layer was identified during the initial data analysis and thus included in the optical model. The model dielectric function (MDF) of all constituents contains contribution from IR optical phonon modes, while the surface-charge-depleted and conductive $In_{0.33}Ga_{0.67}N$ layers contain an additional contribution from free charge carriers. The phonon contribution to the MDF, ε_j^L, is accounted for by[11,15]

$$\varepsilon_j^L = \varepsilon_{\infty,j} \prod_l^k \frac{\omega_{\mathrm{LO},l,j}^2 - \omega^2 - i\omega\gamma_{\mathrm{LO},l,j}}{\omega_{\mathrm{TO},l,j}^2 - \omega^2 - i\omega\gamma_{\mathrm{TO},l,j}}, \tag{1}$$

where $\varepsilon_{\infty,j}$ is the high frequency dielectric constant, k denotes the number of active phonon modes for polarization parallel $j =$ "$\parallel$" (A_1 symmetry) and perpendicular $j =$ "$\perp$" (E_1 symmetry) to the *c*-axis, i is the imaginary unit, ω is the angular frequency, and $\omega_{\mathrm{TO},l,j}$, $\omega_{\mathrm{LO},l,j}$ and $\gamma_{\mathrm{TO},l,j}$, $\gamma_{\mathrm{LO},l,j}$ are the transverse optical phonon (TO) and longitudinal optical phonon (LO) mode frequency and broadening parameters, respectively.

The magnetic field dependent free charge carrier contribution, $\varepsilon_j^{\mathrm{FCC}}$, to the dielectric response of the surface-charge-depleted and conductive $In_{0.33}Ga_{0.67}N$ layers is accounted for by the classical Drude model augmented by the Lorentz force[13,15]

$$\varepsilon_j^{\mathrm{FCC}} = -\boldsymbol{\omega}_{\mathrm{p}}^2 \left(\omega^2 \boldsymbol{I} + i\omega\boldsymbol{\gamma} - i\omega\boldsymbol{\omega}_{\mathrm{c}} \begin{pmatrix} 0 & -b_z & b_y \\ b_z & 0 & -b_x \\ -b_y & b_x & 0 \end{pmatrix} \right)^{-1},$$

where $\boldsymbol{I}$ is the identity matrix, and the magnetic field vector is defined as $\vec{\boldsymbol{B}} = |\vec{\boldsymbol{B}}|(b_x, b_y, b_z)$ in the laboratory coordinate system. At zero magnetic field, the classical Drude contribution is described by the screened plasma frequency tensor, defined as $\boldsymbol{\omega}_{\mathrm{p}}^2 = Nq^2\boldsymbol{m}^{*-1}/(\varepsilon_0\varepsilon_\infty)$, and the plasma broadening tensor $\boldsymbol{\gamma} = q\boldsymbol{\mu}^{-1}\boldsymbol{m}^{*-1}$, which depend on the free charge carrier concentration parameter N, and anisotropic mobility $\boldsymbol{\mu}$ and effective mass $\boldsymbol{m}^*$ tensors (ε_0 is the vacuum dielectric permittivity and q the carrier unit charge). At non-zero magnetic field, the cyclotron frequency tensor appears, $\boldsymbol{\omega}_{\mathrm{c}} = q|\vec{\boldsymbol{B}}|\boldsymbol{m}^{*-1}$, which provides independent access to $\boldsymbol{m}^*$ and the conductivity type ($q = \pm$e, where e is the electron charge and "+" corresponds to p-type while "–" to n-type conductivity). While the zero-field MIR-SE data are sensitive to plasma frequency $\boldsymbol{\omega_p}$ and broadening $\boldsymbol{\gamma}$ parameters and allow

determination of the coupled quantities N/m^* and μm^*, the MIR-OHE data are sensitive to cyclotron frequency ω_c and provide the effective mass parameter. Thus, analysis of the combined MIR-OHE and MIR-SE data allows us to decouple the free charge carrier parameters and obtain independently N, μ, and m^*. The error bars of the experimental data and mismatch between optical model and experimental data contribute to the error bars of the extracted fitting parameters.

The AlN and sapphire MDFs were obtained from previous investigations (Refs. 15 and 16, respectively) and not varied during the analysis. The MDFs of the conductive and the surface charge depletion $In_{0.33}Ga_{0.67}N$ layers shared the same phonon mode contributions with the phonon parameters coupled between the two layers. We found during the MIR-SE data analysis that a MDF containing one TO-LO phonon mode pair for $j =$ "$\perp$" (E_1 symmetry) and one phonon mode pair $j =$ "$\parallel$" (A_1 symmetry) suffices to excellently match the experimental data. This is in agreement with the one phonon mode behavior previously reported for the InGaN A_1(LO) phonon mode from Raman scattering experiments.[17,18] Our result on the one phonon mode behavior of the E_1(TO) presents the experimental confirmation of earlier theoretical predictions using the modified random-element isodisplacement and a rigid-ion model.[19] The TO and LO mode broadening parameters cannot be differentiated in the case of one phonon mode behavior and were thus coupled together in our analysis ($\gamma_{LO,j} = \gamma_{TO,j} = \gamma_j^L$, where $j =$ "$\perp$,$\parallel$"). For wurtzite III-nitride layers with c-plane orientation, SE data are not sensitive to the A_1(TO) phonon parameters.[11] Thus, in the data analysis, the A_1(TO) frequency was set to 504 cm^{-1} according to a linear interpolation between the frequencies for GaN and InN.[1] Due to limited sensitivity, the E_1(LO) phonon frequency $\omega_{LO,\perp}$ was fixed to the linearly interpolated value between the binary parent compounds of 692 cm^{-1}.[1] We further assumed an isotropic high-frequency dielectric constant ($\varepsilon_\infty = \varepsilon_{\infty,\parallel} = \varepsilon_{\infty,\perp}$). The parameters ε_∞ (5.48), the combined thickness ($d = 302$ nm) of the $In_{0.33}Ga_{0.67}N$ depletion and conductive layers, and the AlN layer thickness ($d_{AlN} = 1024$ nm) were determined from analysis of NIR-UV SE measurements and not varied during the MIR-SE and MIR-OHE data analysis. The effective mass and mobility parameters for carrier depleted and conductive layers were allowed to have different values for polarization perpendicular $m_\perp^*$, $\mu_\perp$ and parallel $m_\parallel^*$, $\mu_\parallel$ to the c-axis.

The optical model parameters varied during the MIR-SE and MIR-OHE data analysis were E_1(TO) phonon frequency and broadening ($\omega_{TO,\perp}, \gamma_\perp^L$), A_1(LO) phonon frequency and broadening ($\omega_{LO,\parallel}, \gamma_\parallel^L$), conductive and surface depletion $In_{0.33}Ga_{0.67}N$ layer concentration, mobility and effective mass parameters ($N, m_\perp^*, m_\parallel^*, \mu_\perp, \mu_\parallel$ and $N_{depl}, m_{depl,\perp}^*, m_{depl,\parallel}^*$, $\mu_{depl,\perp}, \mu_{depl,\parallel}$, respectively), and depleted layer thickness parameter (d_{depl}). While the thickness of the surface depletion layer d_{depl} was varied, the combined $In_{0.33}Ga_{0.67}N$ layer thickness was held constant ($d = 302$ nm). The MIR-SE data (Ψ, Δ) and the three MIR-OHE difference datasets [**M**(0 T)-**M**(−6 T), **M**(0 T)-**M**(+6 T), and **M**(+6 T)-**M**(−6 T)], obtained by subtracting MIR-OHE data measured at 6 T, 0 T, and −6 T magnetic fields, were matched simultaneously using the described optical model.

Measured and the best-match model calculated MIR-SE Ψ and Δ spectra at angles of incidence of 55° and 65° are depicted in Fig. 1. An excellent agreement between measured and calculated spectra is observed. The strong feature at around 950 cm^{-1} is assigned to the A_1(LO) phonon coupled to free charge carriers in the conductive $In_{0.33}Ga_{0.67}N$ layer which produce a coupled phonon-plasmon mode. The subtle spectral feature at around 700 cm^{-1} (more apparent in the Ψ spectrum) can only be captured by introducing the surface carrier depleted layer, containing the uncoupled A_1(LO) phonon, in the optical model. This spectral feature is caused by the unscreened A_1(LO) phonon as explained by Kasic *et al.*[11] A similar behavior was observed and explained for Mg-doped InN.[20,21] The broad feature at around 460 cm^{-1} (Fig. 1) can be represented by a weak Lorentz oscillator with polarization perpendicular to the c-axis, a small TO-LO splitting and a large damping parameter, assigned as an impurity mode. Such low-polarity modes were also observed previously in doped GaN and InGaN.[11,22]

Figure 2 depicts experimental and best-match calculated MIR-OHE data in terms of Mueller matrix block off-diagonal elements (ΔM_{ij}, $ij = 13$, 31, 23, and 32) difference data [**M**(0 T)-**M**(−6 T)] between **M**(0 T) and **M**(−6 T) datasets. The other MIR-OHE difference datasets [**M**(0 T)-**M**(+6 T) and **M**(+6 T)-**M**(−6 T)] used in the data analysis are omitted from Fig. 2 for brevity. Note that all block off-diagonal Mueller matrix elements are zero without the external magnetic field, and all differences therefrom are caused by the magnetic-field induced free charge carrier response in the $In_{0.33}Ga_{0.67}N$ layer.

The best-match model parameters for the $In_{0.33}Ga_{0.67}N$ conductive and surface depletion layers are listed in Table I. The electron concentration in the surface depletion layer is found to be below the detection limit of the IR-VASE of

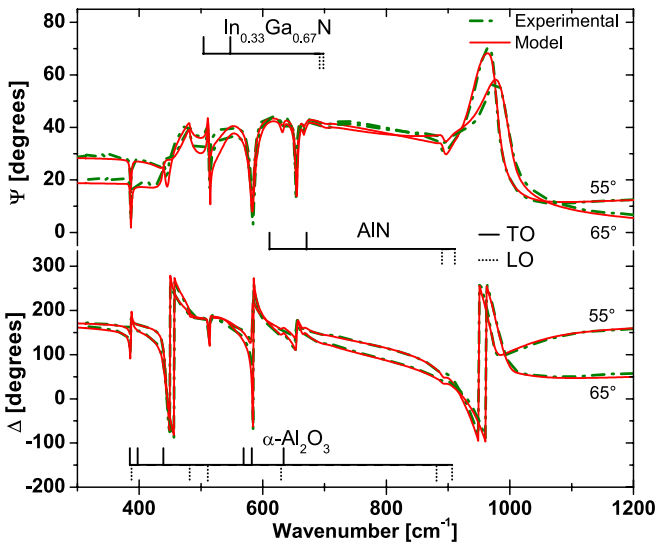

FIG. 1. MIR-SE experimental (solid lines) and the best-match model calculated (dashed-dotted lines) Ψ and Δ spectra for the $In_{0.33}Ga_{0.67}N$ sample. The frequencies of the IR-active optical phonons for TO (solid lines) and LO (dashed lines) in $In_{0.33}Ga_{0.67}N$, AlN, and sapphire are indicated by brackets.

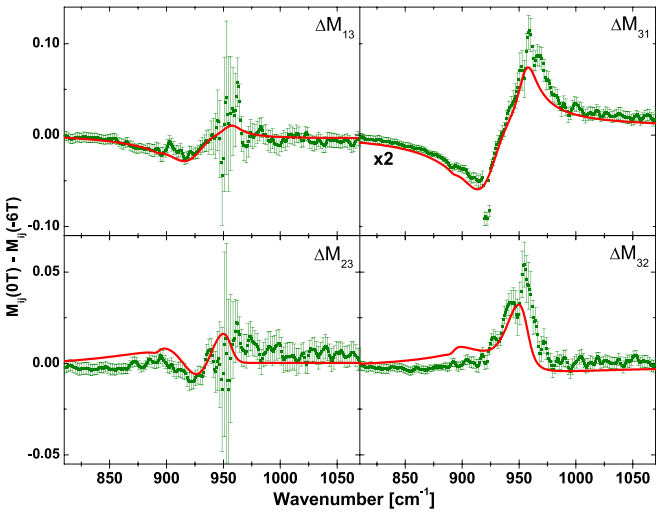

FIG. 2. Experimental (dots) and the best-match model calculated (solid lines) MIR-OHE data, shown as differences between data at zero field and at -6 T [$\mathbf{\Delta M}(-6\,\mathrm{T}) = \mathbf{M}(0\,\mathrm{T}) - \mathbf{M}(-6\,\mathrm{T})$] for elements ΔM_{ij} ($ij = 13$, 31, 23, and 32) for the $In_{0.33}Ga_{0.67}N$ sample.

$10^{17}\,\mathrm{cm}^{-3}$. Thus, the depletion layer has negligible contribution to the OHE signal, and its free charge carrier properties cannot be determined. We note that a surface depletion in $In_xGa_{1-x}N$ films should occur for In contents below $x \approx 0.4$ (in contrast to alloys with $x \geq 0.4$ where surface accumulation was observed),[23,24] which is consistent with our findings. Our MIR-OHE results further revealed n-type conductivity with a free electron concentration of $(1.7 \pm 0.2) \times 10^{19}\,\mathrm{cm}^{-3}$ within the conductive $In_{0.33}Ga_{0.67}N$ layer. A higher mobility is found along the c-axis with $\mu_{\parallel} = 65 \pm 7\,\mathrm{cm}^2/(\mathrm{V\,s})$ and $\mu_{\perp} = 30 \pm 1\,\mathrm{cm}^2/(\mathrm{V\,s})$. A similar anisotropy of the electron mobility parameter was also observed in GaN, InN, and AlGaN alloys and attributed to crystal domains, defect, and impurity distributions in wurtzite-structure, c-plane oriented epitaxial layers.[9,11,15] The best-match-calculated electron effective mass parameters were determined to be $m^*_{\perp} = (0.205 \pm 0.013)\,m_0$ and $m^*_{\parallel} = (0.204 \pm 0.016)\,m_0$. The relative anisotropy of the electron effective mass in InN is $\frac{m^*_{\perp} - m^*_{\parallel}}{m^*_{\perp} + m^*_{\parallel}} \approx 15\%$.[9] Bearing in mind that the electron effective mass in GaN is virtually isotropic,[11] a slight anisotropy is expected for $In_{0.33}Ga_{0.67}N$.

TABLE I. The best-match model parameters obtained from the MIR-SE and MIR-OHE data analysis. Error bars correspond to the 90% confidence interval.

Parameter	Value
$\omega_{TO,\perp}$	$547.3 \pm 0.5\,\mathrm{cm}^{-1}$
$\omega_{LO,\parallel}$	$701 \pm 3\,\mathrm{cm}^{-1}$
$\gamma^L_{\perp}$	$15.9 \pm 0.7\,\mathrm{cm}^{-1}$
$\gamma^L_{\parallel}$	$18 \pm 8\,\mathrm{cm}^{-1}$
N	$(1.7 \pm 0.2) \times 10^{19}\,\mathrm{cm}^{-3}$
$m^*_{\perp}$	$(0.205 \pm 0.013)\,m_0$
$m^*_{\parallel}$	$(0.204 \pm 0.016)\,m_0$
$\mu_{\perp}$	$30 \pm 1\,\mathrm{cm}^2/\mathrm{V\,s}$
$\mu_{\parallel}$	$65 \pm 7\,\mathrm{cm}^2/\mathrm{V\,s}$
N_{depl}	$<10^{17}\,\mathrm{cm}^{-3}$
d_{depl}	$15 \pm 7\,\mathrm{nm}$

However, within our uncertainty limits, no anisotropy of the electron effective mass is detected. We note that the free electron concentration in the $In_{0.33}Ga_{0.67}N$ film of $1.7 \times 10^{19}\,\mathrm{cm}^{-3}$ is relatively high, which may play a role in reducing the anisotropy of the effective mass parameter. It was shown that the anisotropy of the electron effective mass parameter decreases with increasing free electron concentration in InN and vanishes for concentrations above $1 \times 10^{19}\,\mathrm{cm}^{-3}$.[9] Taking into account the error bars of the determined effective mass parameters, we estimate the highest possible relative anisotropy for $In_{0.33}Ga_{0.67}N$ to be $\frac{m^*_{\perp} - m^*_{\parallel}}{m^*_{\perp} + m^*_{\parallel}} \approx 7\%$.

Figure 3 summarizes our results together with previously reported effective mass parameters for InN[9] and GaN.[11] The solid lines indicate the linear interpolation between the isotropically averaged electron effective mass parameters of GaN and InN for different electron concentrations, assuming parabolic bands in GaN and considering the nonparabolicity in InN.[9,25] The GaN value reported by Kasic *et al.*[11] is considered to be independent of the electron concentration.[10] The dependence of the effective mass on the free electron concentration in InN is derived from Kane's two-band $\mathbf{k} \cdot \mathbf{p}$ model[25] where model parameters are obtained by fitting the model to the experimental data reported in Ref. 9. The linear interpolation for the lowest carrier concentration of $10^{15}\,\mathrm{cm}^{-3}$ may be seen as the curvature of the conduction band bottom in $In_xGa_{1-x}N$. The electron effective mass parameter determined in this work is larger

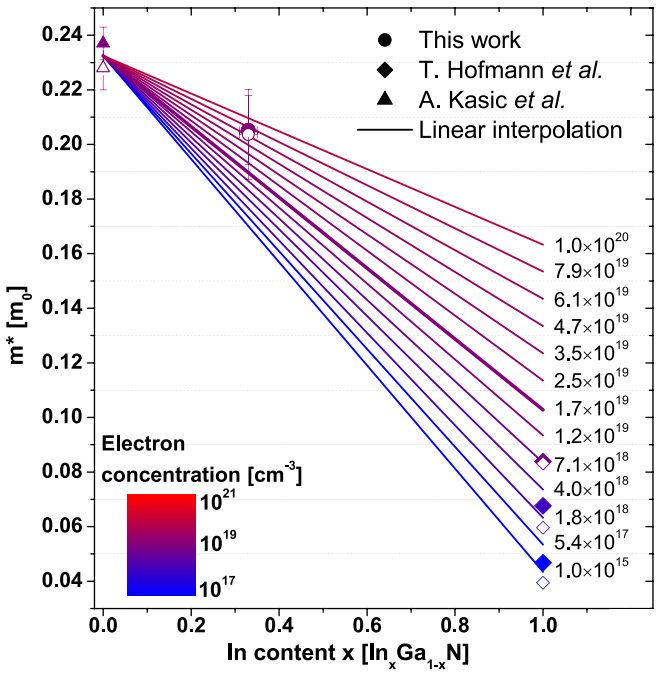

FIG. 3. Electron effective mass parameter in $In_xGa_{1-x}N$ as a function of In content x: MIR-OHE results determined in this work ($\bullet - m^*_{\perp}$, $\circ - m^*_{\parallel}$); InN effective mass from Ref. 9 ($\blacklozenge - m^*_{\perp}$, $\diamond - m^*_{\parallel}$) and GaN effective mass from Ref. 11 ($\blacktriangle - m^*_{\perp}$, $\triangle - m^*_{\parallel}$). The solid lines indicate the dependences of the isotropically averaged $In_xGa_{1-x}N$ electron effective mass parameters on the In content for different electron concentrations obtained from a linear interpolation of the results in Ref. 9 (InN) and Ref. 11 (GaN), considering the nonparabolicity of InN conduction band and assuming full parabolic behavior of GaN conduction band. The color coding represents the free electron concentrations in $In_xGa_{1-x}N$.

than the value at the bottom of the conduction band predicted by the linear interpolation. In principle, this may be due to two effects: (i) a nonparabolic conduction band in the vicinity of the Γ point of $In_{0.33}Ga_{0.67}N$ leading to dependence of the electron effective mass on the carrier concentration and/or (ii) a nonlinear dependence $m^*(x)$ with a significant bowing parameter. A very small effective mass bowing parameter was theoretically predicted for $In_xGa_{1-x}N$.[3] We therefore compare our effective mass parameters with the linear interpolation for the electron concentration in our sample of $1.7 \times 10^{19}\,cm^{-3}$. It can be seen from Fig. 3 that within the error bars, our result is consistent with this linear interpolation and thus indicative for nonparabolicity in $In_{0.33}Ga_{0.67}N$. A larger bowing parameter, however, cannot be ruled out. Further accurate effective mass parameters in $In_xGa_{1-x}N$ with different electron concentrations and different In contents are needed.

In conclusion, the room temperature electron effective mass parameters perpendicular and parallel to the *c*-axis of $In_{0.33}Ga_{0.67}N$ epitaxial layer are determined to be $m^*_\perp = (0.205 \pm 0.013)\,m_0$ and $m^*_\parallel = (0.204 \pm 0.016)\,m_0$ for a free electron concentration of $(1.7 \pm 0.2) \times 10^{19}\,cm^{-3}$. Within our uncertainty limits, the electron effective mass parameter is found to be isotropic and the upper limit of the possible relative anisotropy is estimated to be 7%. Our results indicate that the nonparabolicity of the conduction band in the vicinity of the Γ point of $In_{0.33}Ga_{0.67}N$ is likely present. The free electron mobility is found to be anisotropic with $\mu_\perp = 30 \pm 1\,cm^2/(V\,s)$ and $\mu_\parallel = 65 \pm 7\,cm^2/(V\,s)$. Our results confirm previous experimental and theoretical findings for the one mode behavior of the $A_1(LO)$ phonon and provide experimental support for the theoretical predictions of a one mode behavior of the $E_1(TO)$ phonon in InGaN.

This work was supported by the Swedish Research Council (VR) under Grant No. 2016-00889, the Swedish Governmental Agency for Innovation Systems (VINNOVA) under the VINNMER international qualification program, Grant No. 2011-03486, the Competence Center Program Grant No. 2016-05190, the Swedish Government Strategic Research Area in Materials Science on Functional Materials at Linköping University, Faculty Grant SFO Mat LiU No. 2009-00971, and the Swedish Foundation for Strategic Research (SSF), under Grant Nos. FL12-0181, RIF14-055, and EM16-0024. The authors further acknowledge financial support from the University of Nebraska-Lincoln, the J. A. Woollam Co., Inc., the J. A. Woollam Foundation, and the National Science Foundation (Award Nos. MRSEC DMR 1420645, CMMI 1337856, and EAR 1521428). The authors thank Dr. Mengyao Xie and Professor Dr. Enrique Calleja (Universidad Politécnica de Madrid) for providing the $In_{0.33}Ga_{0.67}N$ sample and Laurent Souqui (Linköping University) for assistance with XRD measurements.

[1]J. Wu, J. Appl. Phys. **106**, 011101 (2009).
[2]L. Ardaravičius, O. Kiprijanovič, J. Liberis, E. Šermukšnis, A. Matulionis, R. A. Ferreyra, V. Avrutin, U. Özgür, and H. Morkoç, Semicond. Sci. Technol. **30**, 105016 (2015).
[3]F. Elfituri and B. Hourahine, Phys. Status Solidi A **209**, 79 (2012).
[4]M. Millot, N. Ubrig, J. M. Poumirol, I. Gherasoiu, W. Walukiewicz, S. George, O. Portugall, J. Léotin, M. Goiran, and J. M. Broto, Phys. Rev. B **83**, 125204 (2011).
[5]B. S. Yadav, P. Mohanta, R. Srinivasa, and S. Major, Thin Solid Films **555**, 179 (2014).
[6]A. Eljarrat, L. Lopez-Conesa, C. Magen, N. Garcia-Lepetit, Z. Gacevic, E. Calleja, F. Peiro, and S. Estrade, Phys. Chem. Chem. Phys. **18**, 23264 (2016).
[7]W. Walukiewicz, J. W. Ager III, K. M. Yu, Z. Liliental-Weber, J. Wu, S. X. Li, R. E. Jones, and J. D. Denlinger, J. Phys. D: Appl. Phys. **39**, R83 (2006).
[8]J. Wu, W. Walukiewicz, W. Shan, K. M. Yu, J. W. Ager, E. E. Haller, H. Lu, and W. J. Schaff, Phys. Rev. B **66**, 201403 (2002).
[9]T. Hofmann, V. Darakchieva, B. Monemar, H. Lu, W. Schaff, and M. Schubert, J. Electron. Mater. **37**, 611 (2008).
[10]M. Feneberg, K. Lange, C. Lidig, M. Wieneke, H. Witte, J. Bläsing, A. Dadgar, A. Krost, and R. Goldhahn, Appl. Phys. Lett. **103**, 232104 (2013).
[11]A. Kasic, M. Schubert, S. Einfeldt, D. Hommel, and T. E. Tiwald, Phys. Rev. B **62**, 7365 (2000).
[12]M. Schubert, T. Hofmann, and C. M. Herzinger, J. Opt. Soc. Am. A **20**, 347 (2003).
[13]M. Schubert, P. Kühne, V. Darakchieva, and T. Hofmann, J. Opt. Soc. Am. A **33**, 1553 (2016).
[14]P. Kühne, C. M. Herzinger, M. Schubert, J. A. Woollam, and T. Hofmann, Rev. Sci. Instrum. **85**, 071301 (2014).
[15]S. Schöche, P. Kühne, T. Hofmann, M. Schubert, D. Nilsson, A. Kakanakova-Georgieva, E. Janzén, and V. Darakchieva, Appl. Phys. Lett. **103**, 212107 (2013).
[16]M. Schubert, T. E. Tiwald, and C. M. Herzinger, Phys. Rev. B **61**, 8187 (2000).
[17]S. Hernández, R. Cuscó, D. Pastor, L. Artús, K. O'Donnell, R. Martin, I. Watson, Y. Nanishi, and E. Calleja, J. Appl. Phys. **98**, 013511 (2005).
[18]J. Ager III, W. Walukiewicz, W. Shan, K. Yu, S. Li, E. Haller, H. Lu, and W. Schaff, Phys. Rev. B **72**, 155204 (2005).
[19]H. Grille, C. Schnittler, and F. Bechstedt, Phys. Rev. B **61**, 6091 (2000).
[20]A. Kasic, M. Schubert, Y. Saito, Y. Nanishi, and G. Wagner, Phys. Rev. B **65**, 115206 (2002).
[21]S. Schöche, T. Hofmann, V. Darakchieva, N. B. Sedrine, X. Wang, A. Yoshikawa, and M. Schubert, J. Appl. Phys. **113**, 013502 (2013).
[22]K. Torii, N. Usukura, A. Nakamura, T. Sota, S. F. Chichibu, T. Kitamura, and H. Okumura, Appl. Phys. Lett. **82**, 52 (2003).
[23]L. R. Bailey, T. D. Veal, P. King, C. F. McConville, J. Pereiro, J. Grandal, M. Sánchez-García, E. Muñoz, and E. Calleja, J. Appl. Phys. **104**, 113716 (2008).
[24]P. King, T. Veal, H. Lu, P. H. Jefferson, S. Hatfield, W. J. Schaff, and C. McConville, Phys. Status Solidi B **245**, 881 (2008).
[25]S. P. Fu and Y. F. Chen, Appl. Phys. Lett. **85**, 1523 (2004).